LETTERS

Disordered, quasicrystalline and crystalline phases of densely packed tetrahedra

Amir Haji-Akbari[1]*, Michael Engel[1]*, Aaron S. Keys[1], Xiaoyu Zheng[3], Rolfe G. Petschek[5], Peter Palffy-Muhoray[4] & Sharon C. Glotzer[1,2]

All hard, convex shapes are conjectured by Ulam to pack more densely than spheres[1], which have a maximum packing fraction of $\phi = \pi/\sqrt{18} \approx 0.7405$. Simple lattice packings of many shapes easily surpass this packing fraction[2,3]. For regular tetrahedra, this conjecture was shown to be true only very recently; an ordered arrangement was obtained via geometric construction with $\phi = 0.7786$ (ref. 4), which was subsequently compressed numerically to $\phi = 0.7820$ (ref. 5), while compressing with different initial conditions led to $\phi = 0.8230$ (ref. 6). Here we show that tetrahedra pack even more densely, and in a completely unexpected way. Following a conceptually different approach, using thermodynamic computer simulations that allow the system to evolve naturally towards high-density states, we observe that a fluid of hard tetrahedra undergoes a first-order phase transition to a dodecagonal quasicrystal[7–10], which can be compressed to a packing fraction of $\phi = 0.8324$. By compressing a crystalline approximant of the quasicrystal, the highest packing fraction we obtain is $\phi = 0.8503$. If quasicrystal formation is suppressed, the system remains disordered, jams and compresses to $\phi = 0.7858$. Jamming and crystallization are both preceded by an entropy-driven transition from a simple fluid of independent tetrahedra to a complex fluid characterized by tetrahedra arranged in densely packed local motifs of pentagonal dipyramids that form a percolating network at the transition. The quasicrystal that we report represents the first example of a quasicrystal formed from hard or non-spherical particles. Our results demonstrate that particle shape and entropy can produce highly complex, ordered structures.

The packing of shapes has drawn the attention of humankind since ancient times. A Sanskrit work from 499 AD reveals the first-known mathematical study of the face-centred cubic arrangement of spheres[11]. Kepler conjectured and Hales only recently proved the sphere-close-packing fraction of $\phi = \pi/\sqrt{18} \approx 0.7405$ achieved by face-centred cubic and its stacking variations[12]. Much less is known about the packing of other shapes. In the case of ellipsoids, periodic arrangements were found with packing fractions up to $\phi = 0.7707$ (ref. 3). The recent progress in the synthesis of non-spherical particles of sizes ranging from nanometres to micrometres[13] has focused attention on the problem of packing three-dimensional shapes such as tetrahedra[14].

In hard particle systems, the potential energy of two particles is considered infinite if they interpenetrate and zero otherwise. All permissible configurations of such systems have the same energy, so the equilibrium structure at constant volume maximizes entropy. Surprisingly, hard particles can maximize entropy by ordering. Entropy-driven disorder–order transitions (first predicted by Onsager[15] for hard thin rods and Kirkwood[16] for hard spheres) are now well established for the originally controversial case of spheres, as well as for rods[17], ellipsoids[18] and other shapes[19,20]. In the limit of infinite pressure, an arrangement with maximum packing fraction is stable because it minimizes specific volume and Gibbs free energy.

One of the simplest shapes for which the packing problem is still unsolved is the regular tetrahedron. Tetrahedra do not tile Euclidean space. However, if extra space is allowed between tetrahedra, or between groups of tetrahedra, dense ordered structures become possible. Imagine building a dense cluster, one tetrahedron at a time. As shown in Fig. 1A, a pentagonal dipyramid is easily built from five tetrahedra if one allows an internal gap of 7.36°. Two pentagonal dipyramids can share a single tetrahedron to form a nonamer. Twelve interpenetrating pentagonal dipyramids define an icosahedron with a gap of 1.54 steradians. In Fig. 1A, tetrahedral dice are stuck together with modelling putty, which distributes the gap that would be present in each motif if most of the adjacent faces were touching. Pentagonal dipyramids and icosahedra are locally dense, but exhibit non-crystallographic symmetries. The problem of extending or arranging them into space-filling bulk structures is non-trivial. For example, adding a second shell to the icosahedron generates a larger cluster with icosahedral symmetry and 70 tetrahedra, but decreases the packing fraction. For later use, we introduce here a dense, one-dimensional packing given by a linear arrangement of tetrahedra with touching faces known as a tetrahelix, or Bernal spiral.

Recent theoretical works have discussed possible ordered phases of hard tetrahedra formed by some of these motifs. Conway and Torquato[21] proposed the Scottish, Irish and Welsh configurations, derived from the polytetrahedral networks of clathrate hydrates with packing fractions of up to $\phi = 0.7175$. Chen[4] constructed a crystalline structure formed from nonamers with $\phi = 0.7786$, the first to exceed sphere close packing, and showing that tetrahedra obey Ulam's conjecture. Chen's structure was subsequently compressed to $\phi = 0.7820$ (ref. 5) and the same algorithm applied to different initial conditions yielded $\phi = 0.8230$ (ref. 6). All these packings originated from either geometric considerations or numerical compression. No simulation or experiment has yet reported the spontaneous formation of an ordered phase of hard tetrahedra. Aside from studies of packing, hard tetrahedra have been used to model the structure of water[22]. Polytetrahedral networks of atoms are characteristic for Frank–Kasper phases[23], common in intermetallic compounds.

To obtain dense packings of hard regular tetrahedra, we carry out Monte Carlo simulations. Figure 1B–D shows the densest configuration ($\phi = 0.8324$) we obtained: we equilibrated an initially disordered fluid of 13,824 tetrahedra at constant $\phi = 0.5$ and then we compressed the ordered structure that forms. As demonstrated below, this structure is a quasicrystal, with a packing fraction much greater than all previously proposed arrangements of regular tetrahedra. First, we discuss the thermodynamics of the hard tetrahedron fluid.

[1]Department of Chemical Engineering, [2]Department of Materials Science and Engineering, University of Michigan, Ann Arbor, Michigan 48109, USA. [3]Department of Mathematical Sciences, [4]Liquid Crystal Institute, Kent State University, Kent, Ohio 44242, USA. [5]Department of Physics, Case Western Reserve University, Cleveland, Ohio 44106, USA.
*These authors contributed equally to this work.

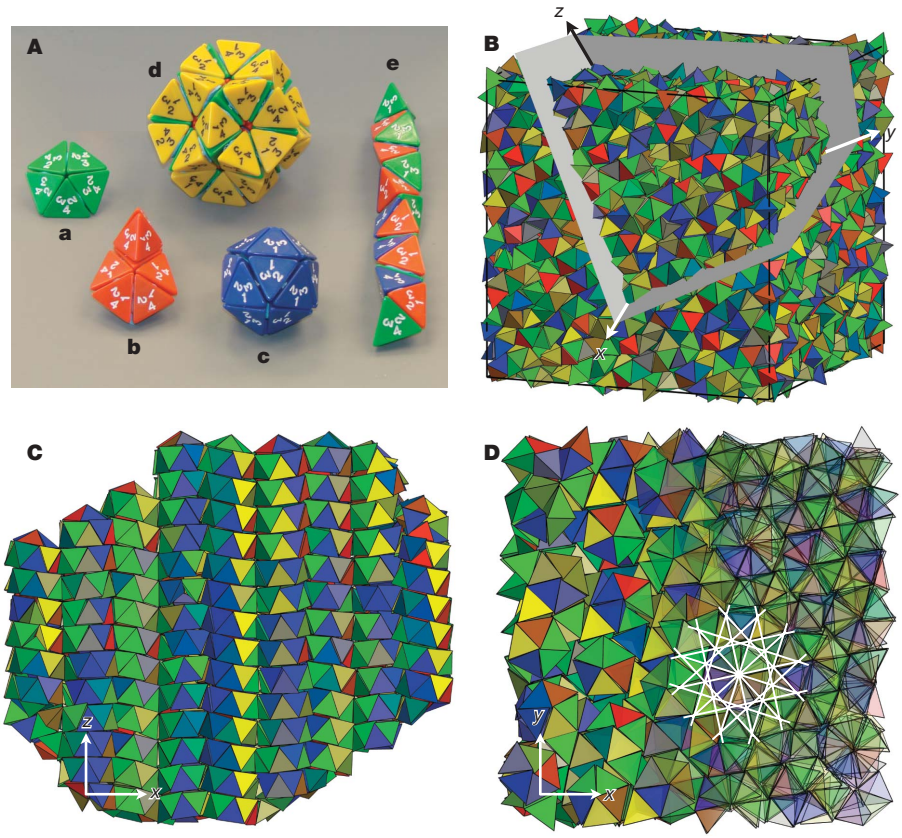

Figure 1 | Packings of tetrahedra obtained by hand and by computer simulation. **A**, Ideal local packing motifs built from tetrahedral dice stuck together with modelling putty. The pentagonal dipyramid (**a**), the nonamer (**b**) and the icosahedron (**c**) maximize local packing density. The icosahedron can be extended by adding a second shell (**d**), but then the large gaps between the outer tetrahedra lower the density. The tetrahelix (**e**) maximizes packing density in one dimension. **B**–**D**, A quasicrystal with packing fraction $\phi = 0.8324$ obtained by first equilibrating an initially disordered fluid of 13,824 hard tetrahedra using Monte Carlo simulation and subsequent numerical compression. The images show an opaque view of the system (**B**) and opaque and translucent views of two rotated narrow slices **C** and **D**. The white overlay in **D** shows the distinctive 12-fold symmetry of the dodecagonal quasicrystal. Corrugated layers with normals along the z axis are apparent in **C**. The colouring of the tetrahedra is based on orientation.

Figure 2a shows the equation of state $\phi(P^*)$ obtained from simulations of a small system with 512 tetrahedra and a larger system with 4,096 tetrahedra. Here, $P^* = P\sigma^3/k_BT$ is the reduced pressure and σ the edge length of a tetrahedron. For the small system, the equilibrium packing fraction exhibits an S-shaped transition at $P^* = 58$ and $\phi = 0.47$ from a simple fluid to a more complex fluid, discussed below. At higher pressure the system jams (Supplementary Figs 1 and 2) and, when compressed to nearly infinite pressure, attains a maximum packing fraction of $\phi = 0.7858$. The large system undergoes a first-order transition on compression of the fluid phase and forms a quasicrystal. In Fig. 2b, we analyse the system for the presence of locally dense motifs introduced in Fig. 1A. We see that the fraction of tetrahedra belonging to at least one pentagonal dipyramid increases well before jamming or crystallization. With increasing pressure, interpenetrating pentagonal dipyramids form icosahedra and finally merge into a percolating pentagonal dipyramid network (Fig. 2c, d) as the fraction of tetrahedra in pentagonal dipyramids approaches unity. For the large system, the fraction of tetrahedra in icosahedra suddenly drops at $P^* = 62$, when crystallization occurs. Comparison with the glass shows that far fewer icosahedra remain in the quasicrystal. Figure 2c and d suggests a percolation transition of the pentagonal dipyramid network in both systems at $P^*_p = 58 \pm 2$, before both jamming and crystallization. We do not observe tetrahedratic liquid crystal phases, which have been suggested by theory[24].

Structural changes in the fluid are revealed by the unusual behaviour of its radial distribution function $g(r)$, as shown in Fig. 2e. We find that the first peak near $r = 0.75\sigma$ disappears upon compression at low pressure, only to reappear for higher pressure, splitting into two peaks at $r = 0.55\sigma$ and $r = 0.80\sigma$. The positions of these peaks are characteristic of face-to-face and edge-to-edge arrangements, respectively, within a single pentagonal dipyramid. This initial loss of structure with increasing pressure or packing fraction is strikingly different from the well-known behaviour of the hard sphere system depicted in Fig. 2f, and underscores the influence of shape in dense packings.

The spontaneous formation of a quasicrystal from the fluid is remarkable since all previously observed crystalline structures of hard particles have unit cells consisting of only a few particles[17,19,20]. From Fig. 1C it can be seen that the quasicrystal consists of a periodic stack of corrugated layers with spacing 0.93σ. The view along the direction of the stacking vector (Fig. 1D) reveals details of the structure within the layers. Twelve-fold symmetric rings formed by interpenetrating tetrahelices exist throughout the structure. The helix chirality is switched by 30° rotations, lowering the symmetry and resulting in a generalized point group of D_{6d} (ref. 25).

The structure of the quasicrystal can be understood more easily by examining the dual representation constructed by connecting the centres of mass of neighbouring tetrahedra. In the dual representation, pentagonal dipyramids are represented by pentagons. The mapping is applied to a layer of an 8,000-particle quasicrystal in Fig. 3a. Recurring motifs are rings of twelve tetrahedra that are stacked periodically to form 'logs' (Fig. 3b), similar to the hexagonal antiprismatic clusters in the tantalum–tellurium system[10]. As indicated in Fig. 3a, the symmetry axes of the logs arrange into a non-repeating pattern of squares and triangles (tile edge length 1.83σ)—an observation that we confirm

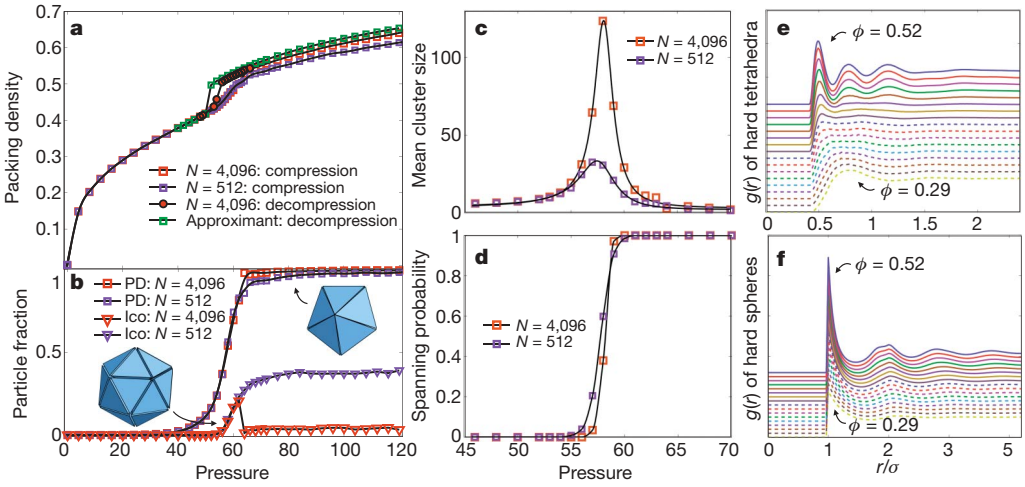

Figure 2 | Thermodynamic and structural properties of the hard tetrahedron fluid. **a**, Equation of state spanning the transition from the liquid to the solid state. Data are shown for various system sizes. Decompression of both the quasicrystal ($N = 4{,}096$) and the approximant (unit cell $N = 82$) shows a sharp melting transition. Hysteresis of the compression and decompression curves for the quasicrystal further indicates a first-order transition. For the system with $N = 512$, crystallization is inhibited in many runs, producing a jammed, disordered glass. **b**, Fraction of tetrahedra participating in pentagonal dipyramids ('PD', right inset) and icosahedra ('Ico', left inset). **c**, Mean cluster size of interpenetrating pentagonal dipyramids. **d**, Spanning probability of the largest cluster of interpenetrating pentagonal dipyramids. **e**, Radial distribution function $g(r)$ of regular tetrahedra for packing fractions ranging from $\phi = 0.29$ to $\phi = 0.52$. Curves are vertically offset for clarity. **f**, Radial distribution function for the same densities as in **e** for a hard sphere system.

in systems with 13,824 and 21,952 particles (Supplementary Figs 3 and 4). The diffraction pattern obtained by positioning scatterers at the centres of tetrahedra shows rings of Bragg peaks, indicating the presence of long-range order with 12-fold symmetry not compatible with periodicity. Perfect quasicrystals are aperiodic while extending to infinity; they therefore cannot be realized in experiments or simulations, which are, by necessity, finite. The observed tilings and diffraction patterns with 12-fold symmetry are sufficient in practice for the identification of our self-assembled structures as dodecagonal quasicrystals. Such an identification is in agreement with previous theoretical analysis of random square-triangle tilings[26] and findings of dodecagonal quasicrystals in recent experiments[7–10] and simulations[27,28].

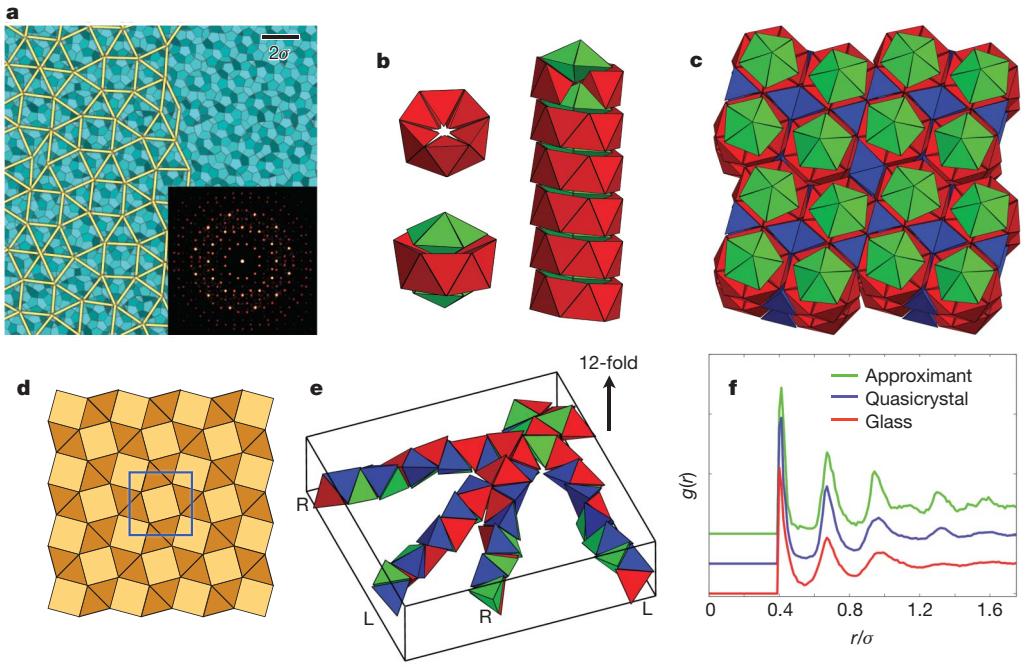

Figure 3 | Structural characterization of the hard tetrahedra dodecagonal quasicrystal and its approximant. **a**, Network of connected tetrahedra in a slice through a quasicrystal with 8,000 tetrahedra, viewed along the direction of the 12-fold axis. Lines connecting the centre of mass of nearest-neighbour tetrahedra form turquoise pentagons, which correspond to the pentagonal dipyramid network. The tiling structure is highlighted in yellow. A diffraction pattern indicating 12-fold symmetry is shown in the inset. **b**, The vertices of the tiling are formed by logs comprised of rings of twelve tetrahedra, with neighbouring rings enclosing a pentagonal dipyramid. The packing fraction within the logs can be increased by a tilt of the rings with respect to the log axis. This allows neighbouring pentagonal dipyramids to avoid each other, as indicated in the figure, where two tetrahedra have been removed from the top ring to expose pentagonal dipyramids. **c**, **d**, Structure (**c**) and tiling (**d**) of the $(3,4,3^2,4)$ approximant to the dodecagonal quasicrystal of tetrahedra. Colours are described in the main text. **e**, Similar to the quasicrystal, interpenetrating tetrahelices are present throughout the approximant. Their chirality alternates between left (L) and right (R) by 30° rotations. **f**, Radial distribution functions for the approximant ($N = 82$), quasicrystal ($N = 8{,}000$), and glass ($N = 8{,}000$). Curves are vertically offset for clarity.

Quasicrystal approximants are periodic crystals with local tiling structure identical to that in the quasicrystal[25]. Because they are closely related, and are often observed in experiments, we consider them as candidates for dense packings. The dodecagonal approximant with the smallest unit cell (space group $P\bar{4}n2$) has 82 tetrahedra (Fig. 3c) and corresponds to one of the Archimedean tilings[29]. At each vertex we see the logs of twelve-member rings (shown in red) capped by single pentagonal dipyramids (green). The logs pack well into squares and triangles with additional, intermediary tetrahedra (blue). The vertex configuration of the tiling is $(3,4,3^2,4)$, as shown in Fig. 3d. Interpenetrating tetrahelices can also be seen in the approximant (Fig. 3e). 'Building' and numerically compressing a unit cell of this ideal structure achieves a packing fraction of $\phi = 0.8479$. If we compress a $2 \times 2 \times 2$ unit cell, the packing fraction marginally increases to $\phi = 0.8503$, the densest packing of tetrahedra yet reported (Supplementary Figs 5 and 6). Compressing approximants with more complex unit cells, more faithful to an ideal quasicrystal, does not further improve the packing (Supplementary Fig. 7), which suggests that a $(3,4,3^2,4)$ crystal is the thermodynamically preferred phase at higher pressures.

The fact that the dodecagonal quasicrystal routinely forms in isochoric Monte Carlo simulations of fluids at packing fractions $\phi \geq 0.5$ indicates that the quasicrystal is thermodynamically favoured over the fluid at intermediate pressures. Whether it is stable or metastable relative to the approximant at these pressures is unclear, because the higher entropy of the quasicrystal competes with the higher density of the $(3,4,3^2,4)$ approximant (Fig. 2a) to minimize the Gibbs free energy, and entropically stabilized quasicrystals are known to exist[30,31]. Nonetheless, because the transformation to an approximant is a very slow process[26], the dodecagonal quasicrystal might be 'practically' stable, even if it is not the thermodynamically stable phase.

Why should square-triangle tilings be preferred for dense packings of tetrahedra? First, we compare the packing fraction of the square tile (22 tetrahedra) to that of the triangle tile (9.5 tetrahedra). Their ratio $\phi_{\text{triangle}}/\phi_{\text{square}} = 19/11\sqrt{3} \approx 0.9972$ is nearly unity, which suggests that tetrahedra pack equally well in both tiles. Second, we note that rings comprising the logs are tilted (Fig. 3b and Supplementary Fig. 8) and the layers of the structure are corrugated (Fig. 1C). This is a direct consequence of the face-to-face packing of tetrahedra where neighbouring logs kiss. As a result, the square tile has a negative Gaussian curvature whereas the triangle tile has a positive one. Alternating the two tiles produces a net zero curvature in the layers, as observed in the quasicrystal and its approximant.

As shown in Fig. 3f, the local structures of the $(3,4,3^2,4)$ approximant, the dodecagonal quasicrystal and the disordered glass (as characterized by their radial distribution functions) are very similar. The peak positions are identical: only the peak heights differ. This implies that the local structure of the glass and quasicrystal are only subtly different, and more sensitive measures of local order, as in Fig. 2b, are required. The crucial step during crystallization is the transformation of the percolating pentagonal dipyramid network into layers, and the elimination of icosahedra. This intriguing process will be investigated in subsequent studies.

In conclusion, we report the highest-known packing fraction of regular tetrahedra and show unexpected ways in which they can pack more densely than previously proposed, including the first quasicrystal formed from non-spherical particles. The spontaneous formation of a quasicrystal of hard particles demonstrates that shape alone can produce remarkable structural complexity through solely entropic interactions.

METHODS SUMMARY

We use isobaric and isochoric Monte Carlo simulations with periodic boundary conditions to study systems of N regular tetrahedra, with N ranging from 512 to 21,952. A full Monte Carlo cycle consists of $N + 1$ trial moves including translation plus rotation of a tetrahedron or rescaling of the orthorhombic box. Maximum step sizes are updated occasionally to keep the acceptance probabilities at 30%. Simulations are initialized at low packing fraction in a random configuration and subsequently compressed to higher densities. The dodecagonal quasicrystals shown in Figs 1 and 3 and Supplementary Figs 1, 3 and 4 are obtained in isochoric simulations at packing fraction $\phi = 0.5$. Crystallization proceeds in three steps: (1) equilibration of the dense, metastable fluid (for example, $N = 8{,}000$: $<12 \times 10^6$ Monte Carlo cycles); (2) nucleation and growth ($12–23 \times 10^6$ Monte Carlo cycles); and (3) healing of defects ($>23 \times 10^6$ Monte Carlo cycles). The equation of state in Fig. 2a is calculated by increasing (or decreasing) the external pressure step-wise for compression (or decompression). Longer simulations facilitate equilibration in the transition region. For detecting pentagonal dipyramids and icosahedra in Fig. 2b, nearest neighbours are sampled with a distance cut-off of 0.65σ. The resulting motifs are further screened by projecting the directions of the tetrahedra onto the surface of the unit sphere, and indexing the resulting pattern using spherical harmonics and comparison with an ideal pattern (a pentagon for a pentagonal dipyramid and a dodecahedron for an icosahedron). For $P^* > 120$, compression with conventional Monte Carlo is inefficient. Therefore we apply an alternative method to reach pressures as large as $P^* \geq 10^6$ and obtain maximum-density packings. The method relies on allowing a small number (of the order of 0.1% of all particles) of minor overlaps (interpenetration of tetrahedra) during box rescaling. All overlaps are subsequently eliminated with isochoric Monte Carlo. Details of our algorithms and the particle data are given in the online-only Methods.

Note added in proof: A new result by Kallus *et al.*[32] indicates a dimer crystal with a packing fraction of $100/117 \approx 0.8547$.

Full Methods and any associated references are available in the online version of the paper at www.nature.com/nature.

Received 5 July; accepted 3 November 2009.

1. Gardner, M. *The Colossal Book of Mathematics: Classic Puzzles, Paradoxes, and Problems* 135 (Norton, 2001).
2. Betke, U. & Henk, M. Densest lattice packings of 3-polytopes. *Comput. Geom.* **16,** 157–186 (2000).
3. Donev, A., Stillinger, F. H., Chaikin, P. M. & Torquato, S. Unusually dense crystal packing of ellipsoids. *Phys. Rev. Lett.* **92,** 255506 (2004).
4. Chen, E. R. A dense packing of regular tetrahedra. *Discrete Comput. Geom.* **40,** 214–240 (2008).
5. Torquato, S. & Jiao, Y. Dense packings of the Platonic and Archimedean solids. *Nature* **460,** 876–879 (2009).
6. Torquato, S. & Jiao, Y. Dense packings of polyhedra: Platonic and Archimedean solids. *Phys. Rev. E* **80,** 041104 (2009).
7. Zeng, X. *et al.* Supramolecular dendritic liquid quasicrystals. *Nature* **428,** 157–160 (2004).
8. Hayashida, K., Dotera, T., Takano, A. & Matsushita, Y. Polymeric quasicrystal: mesoscopic quasicrystalline tiling in ABC star polymers. *Phys. Rev. Lett.* **98,** 195502 (2007).
9. Talapin, D. V. *et al.* Quasicrystalline order in self-assembled binary nanoparticle superlattices. *Nature* **461,** 964–967 (2009).
10. Conrad, M., Krumeich, F. & Harbrecht, B. A dodecagonal quasicrystalline chalcogenide. *Angew. Chem. Int. Ed.* **37,** 1384–1386 (1998).
11. Hales, T. C. Historical overview of the Kepler conjecture. *Discrete Comput. Geom.* **36,** 5–20 (2006).
12. Hales, T. C. A proof of the Kepler conjecture. *Ann. Math.* **162,** 1065–1185 (2005).
13. Glotzer, S. C. & Solomon, M. J. Anisotropy of building blocks and their assembly into complex structures. *Nature Mater.* **6,** 567–572 (2007).
14. Tang, Z. Y., Zhang, Z. L., Wang, Y., Glotzer, S. C. & Kotov, N. A. Spontaneous self-assembly of CdTe nanocrystals into free-floating sheets. *Science* **314,** 274–278 (2006).
15. Onsager, L. The effect of shape on the interaction of colloidal particles. *Ann. NY Acad. Sci.* **51,** 627–659 (1949).
16. Kirkwood, J. E. in *Phase Transformations in Solids* (eds Smoluchowski, R., Mayer, J. E. & Weyl, W. A.) 67 (Wiley, 1951).
17. Bolhuis, P. & Frenkel, D. J. Tracing the phase boundaries of hard spherocylinders. *J. Chem. Phys.* **106,** 666–687 (1997).
18. Camp, P. J. & Allen, M. P. Phase diagram of the hard biaxial ellipsoid fluid. *J. Chem. Phys.* **106,** 6681–6688 (1997).
19. Veerman, J. A. C. & Frenkel, D. Phase-behavior of disk-like hard-core mesogens. *Phys. Rev. A* **45,** 5632–5648 (1992).
20. John, B. S., Juhlin, C. & Escobedo, F. A. Phase behavior in colloidal hard perfect tetragonal parallelepipeds. *J. Chem. Phys.* **128,** 044909 (2009).
21. Conway, J. H. & Torquato, S. Packing, tiling and covering with tetrahedra. *Proc. Natl Acad. Sci. USA* **103,** 10612–10617 (2006).
22. Kolafa, J. & Nezbeda, I. The hard tetrahedron fluid: a model for the structure of water. *Mol. Phys.* **84,** 421–434 (1994).
23. Frank, F. C. & Kasper, J. S. Complex alloy structures regarded as sphere packings. 1. Definitions and basic principles. *Acta Crystallogr.* **11,** 184–190 (1958).
24. Fel, L. G. Tetrahedral symmetry in nematic liquid crystals. *Phys. Rev. E* **52,** 702–717 (1995).
25. Yamamoto, A. Crystallography of quasiperiodic crystals. *Acta Crystallogr. A* **52,** 509–560 (1996).
26. Oxborrow, M. & Henley, C. L. Random square-triangle tilings—a model for twelvefold-symmetrical quasi-crystals. *Phys. Rev. B* **48,** 6966–6998 (1993).

27. Roth, J. & Denton, A. R. Solid-phase structures of the Dzugutov pair potential. *Phys. Rev. E* **61,** 6845–6857 (2000).
28. Keys, A. S. & Glotzer, S. C. How do quasicrystals grow? *Phys. Rev. Lett.* **99,** 235503 (2007).
29. Mikhael, J., Roth, J., Helden, L. & Bechinger, C. Archimedean-like tiling on decagonal quasicrystalline surfaces. *Nature* **454,** 501–504 (2008).
30. Steurer, W. Structural phase transitions from and to the quasicrystalline state. *Acta Crystallogr. A* **61,** 28–38 (2005).
31. Engel, M. & Trebin, H.-R. Self-assembly of complex crystals and quasicrystals with a double-well interaction potential. *Phys. Rev. Lett.* **98,** 225505 (2007).
32. Kallus, Y., Elser, V. & Gravel, S. A dense periodic packing of tetrahedra with a small repeating unit. Preprint at ⟨http://arxiv.org/abs/0910.5226⟩ (2009).

Supplementary Information is linked to the online version of the paper at www.nature.com/nature.

Acknowledgements The Air Force Office of Scientific Research supported A.H.-A., P.P.-M. and S.C.G. The National Science Foundation supported A.S.K., A.H.-A. and S.C.G. in the shape-matching analyses that identified local motifs. M.E. was supported by a postdoctoral fellowship of the Deutsche Forschungsgemeinschaft.

Author Contributions A.H.-A. and M.E. performed all simulations and contributed equally to the study. M.E. solved the quasicrystal and approximant structures. A.S.K. performed shape-matching analysis. X.Z., P.P.-M., and R.G.P. proposed and constructed geometric packings. All authors discussed and analysed the results, and contributed to the scientific process. S.C.G., A.H.-A., and M.E. wrote most of the paper, and all authors contributed to refinement of the manuscript. S.C.G. and P.P.-M. conceived and designed the study, and S.C.G. directed the study.

Author Information Reprints and permissions information is available at www.nature.com/reprints. Correspondence and requests for materials should be addressed to S.C.G. (sglotzer@umich.edu).

METHODS

We define an ideal, regular tetrahedron as the convex hull of its four vertices $v_1 = (1,1,1)$, $v_2 = (1,-1,-1)$, $v_3 = (-1,1,-1)$, $v_4 = (-1,-1,1)$. The edge length of the tetrahedron is $\sigma = \sqrt{8}$ and its volume $V_t = 8/3$. The position and orientation of an arbitrary tetrahedron is given by (x, y, z, a, b, c, d), where (x, y, z) is the translation vector and (a, b, c, d) a quaternion describing the rotation. The relation between the quaternion and the rotation matrix is:

$$R = \begin{pmatrix} a^2+b^2-c^2-d^2 & 2(bc-ad) & 2(bd+ac) \\ 2(bc+ad) & a^2-b^2+c^2-d^2 & 2(cd-ab) \\ 2(bd-ac) & 2(cd+ab) & a^2-b^2-c^2+d^2 \end{pmatrix}$$

Overlap detection. Individual Monte Carlo moves consist of small rotation steps and translation steps with translation vectors chosen randomly in a cubic box of edge length Δr. The most time-consuming part of our algorithm is the overlap check. Tetrahedra are sorted into a cell list with cell size $2\sqrt{3}$, which is the distance beyond which two tetrahedra cannot overlap. Two different overlap detection algorithms are used. They have been designed, written, and tested independently by different co-authors of the present work. Comparing the results of the algorithms on a test set with overlapping and non-overlapping tetrahedra allows independent verification of the codes. The numerical precision of the overlap detection algorithm and therefore the reported packing densities is standard double floating-point precision.

The first algorithm is based on the observation that two convex polyhedra overlap, if and only if at least one edge of one polyhedron intersects one face of the other polyhedron. This means that maximally $2 \times 6 \times 4 = 48$ intersections of lines and triangles have to be evaluated. The algorithm can be optimized by sorting the vertices of each tetrahedron based on their distance from the centre of the other tetrahedron. Only the three edges among the three closest vertices for each tetrahedron require inspection. Additionally, the face that does not include the nearest of the vertices can be discarded. This reduces the necessary checks to a maximum of 18.

The second, independent algorithm takes advantage of the fact that two convex polyhedra do not intersect if and only if a plane can be found that completely separates them. In other words, the vertices of one tetrahedron must lie on one side of the plane and the vertices of the other tetrahedron on the other side. Taking two vertices of one tetrahedron and one vertex of the other tetrahedron defines a trial candidate for a separating plane. It can be shown that the study of all such trial candidates is sufficient. Thus, $6 \times 2 \times 2 = 24$ trial candidates need to be checked. Similar to the first algorithm, sorting the vertices allows reduction in the number of candidates. For production simulation runs we use the second overlap detection algorithm only because it is more efficient than the first algorithm.

Compression algorithm. To obtain the maximum density for a given configuration, we quickly compress to very high densities a system first equilibrated using standard isobaric or isochoric Monte Carlo. Such rapid compression is inefficient with the standard isobaric Monte Carlo scheme, so we use a modified Monte Carlo scheme. Our modified scheme is only used to obtain high-density results; the conventional isochoric and isobaric Monte Carlo methods are used to produce equation-of-state data and to produce the quasicrystals and jammed structures from the fluid.

In the conventional isobaric Monte Carlo algorithm for hard particles, trial volume changes are performed by rescaling the box dimensions. If such a volume change creates an overlap it is discarded, otherwise it is accepted according to the Metropolis criterion for the isobaric ensemble. As the density increases, trial compression moves generate overlaps with larger and larger probability, especially for big systems, making conventional isobaric Monte Carlo slow in equilibrating high densities. To compress our system more efficiently, we introduce a modified scheme that allows a few minor overlaps during compression; these overlaps are then removed to obtain the final configuration.

For our modified scheme, we always accept volume changes, even if they create overlaps. To ensure that the number and amount of overlaps remains small, we use a separate criterion to decide whether the box should be expanded or compressed. We keep track of the acceptance probability p of Monte Carlo translation moves and compare this to a target acceptance probability $p_0 = 0.3$. If $p < p_0$, we apply a compression move, otherwise we apply an expansion move. For our system, we find that rescaling of the box dimensions by a random factor between 1 and $1 + 0.002\Delta r$ for expansion and a random factor between $1 - 0.002\Delta r$ and 1 for compression gives a good balance between fast compression and creating overlaps that are small enough to remove later. The average fraction of particles that overlap during compression is very small, on the order of 0.1% of all particles.

The control parameter for our 'high-density' compression algorithm is the maximum distance of Monte Carlo translation moves, Δr. Although it is not possible to directly measure or control the pressure in our method, we observe that a lower value of Δr corresponds to a higher pressure. For maximum compression, Δr is lowered exponentially to zero.

Our method is extremely simple, fast and robust. By running a short isochoric simulation at the end, we rapidly remove any pre-existing overlaps. This involves implementing the standard translation and rotation Monte Carlo moves, which guarantees that no new overlaps are created and allows sufficient motion, even at very high densities. Using the two independent overlap detection algorithms described above, we ensure that all overlaps are removed for the data reported in this Letter.

Performance. On a single central processing unit (CPU) core, the run time for our most efficient overlap detection scheme is about 5 μs per particle per Monte Carlo cycle at an intermediate packing density. Typical compression runs for the 13,824 tetrahedra system take a few hours on a single AMD Opteron CPU core with 2.3-GHz clock speed. To obtain good candidates with maximum densities we extended the compression time to a few days. Because of these finite compression times, we restrict the packing densities given in the text to four significant digits. Nucleating the quasicrystal from the fluid in an isochoric simulation and then compressing the quasicrystal with 13,824 particles over 40 million Monte Carlo cycles using our compression algorithm to achieve the data shown in Fig. 1B–D took about one month on a single CPU core.